Journal of Glaciology, Vol. 44, No. 146, 1998

Radar reflections reveal a wet bed beneath stagnant Ice Stream C and a frozen bed beneath ridge BC, West Antarctica

C. R. Bentley, N. Lord, C. Liu
Geophysical and Polar Research Center, University of Wisconsin–Madison, Madison, Wisconsin 53706, U.S.A.

ABSTRACT. Digital airborne radar data were collected during the 1987–88 Antarctic field season in nine gridded blocks covering the downstream portions of Ice Stream B (6 km spacing) and Ice Stream C (11 km spacing), together with a portion of ridge BC between them. An automated processing procedure was used for picking onset times of the reflected radar pulses, converting travel times to distances, interpolating missing data, converting pressure transducer readings, correcting navigational drift, performing cross-over analysis, and zeroing remanent crossover errors. Interpolation between flight-lines was carried out using the minimum curvature method.

Maps of ice thickness (estimated accuracy 20 m) and basal-reflection strength (estimated accuracy 1 dB) were produced. The ice-thickness map confirms the characteristics of previous reconnaissance maps and reveals no new features. The reflection-strength map shows pronounced contrasts between the ice streams and ridge BC and between the two ice streams themselves. We interpret the reflection strengths to mean that the bed of Ice Stream C, as well as that of Ice Stream B, is unfrozen, that the bed of ridge BC is frozen and that the boundary between the frozen bed of ridge BC and the unfrozen bed of Ice Stream C lies precisely below the former shear margin of the ice stream.

INTRODUCTION

During the 1987–88 field season of the Siple Coast Project we collected 17 000 km of airborne radar data along a grid of flight-lines, regularly spaced 6 or 11 km apart, on nine blocks over the downstream portions of Ice Streams B and C (Fig. 1; the ice-stream boundaries shown in all the figures, taken from Shabtaie and Bentley (1988), were mapped from widely spaced reconnaissance flights primarily on the basis of heavy crevassing as evinced by strong radar backscatter). In this paper we discuss the collection, reduction and interpretation of these data, which have resulted in an accurate and detailed map of ice thickness and the first map of basal-reflection strength for the area.

RADAR SYSTEM

We used a modified SPRI Mark IV 50 MHz transceiver (Schultz and others, 1987) that transmits a 300 ns pulse with a peak envelope power of 500 W at a rate of 750 pulses s^{-1}. It was mounted in a De Havilland Twin Otter aircraft along with an antenna system that comprised two folded dipoles encased in airfoil-shaped housings and mounted 1/4 wavelength (1.5 m) under the wings (Shabtaie and Bentley, 1987). The aircraft was equipped with a Litton LTN72 inertial navigation system (INS), a Sperry radar altimeter (model 200) and a Rosemount pressure transducer. The digital recording system was described by Retzlaff and others (1993).

SURVEY-GRID DESIGN AND DATA COLLECTION

Eight of the nine blocks (a–h) (Fig. 2) were flown in both the transverse (perpendicular to ice-stream flow) and longitudinal (parallel to ice-stream flow) directions. The 17 000 km of airborne radar profiling were collected during 32 4 h flights. Flight-lines were spaced 6 km apart over Ice Stream B (blocks a–f) and Crary Ice Rise (block i; transverse lines only) and 11 km apart over Ice Stream C (blocks g and h). One raw and one 512-trace stack were recorded every 60 m.

DATA REDUCTION

Approximately 1.4 GB of data were collected. The principal characteristics of the data-reduction procedures were given by Retzlaff and others (1993); here we give only a brief summary. The arrival times of the surface and basal reflections were picked by an auto-picker developed in-house. Ice thicknesses were calculated from the difference between basal and surficial reflection times using an average velocity for electromagnetic waves in the ice sheet of 171 m μs^{-1}, equivalent (for an ice sheet 1000 m thick) to using a velocity in solid ice of 169 m μs^{-1} and adding 10 m to correct for the low-density firn (cf. Shabtaie and Bentley, 1988). We have not attempted to discriminate between reflection hyperbolae and real basal echoes; no migration corrections have been applied. Short data gaps were filled in by interpolation based on a least-squares straight-line fit to the five nearest data points on each side of the gap. Larger gaps were filled by fitting a second-order polynomial to the surrounding points by least squares, using a weighting function that emphasizes high signal-to-noise ratio records and records near the gap.

Navigation

Positional accuracy along each flight was limited by inertial

https://doi.org/10.3189/S0022143000002434 Published online by Cambridge University Press

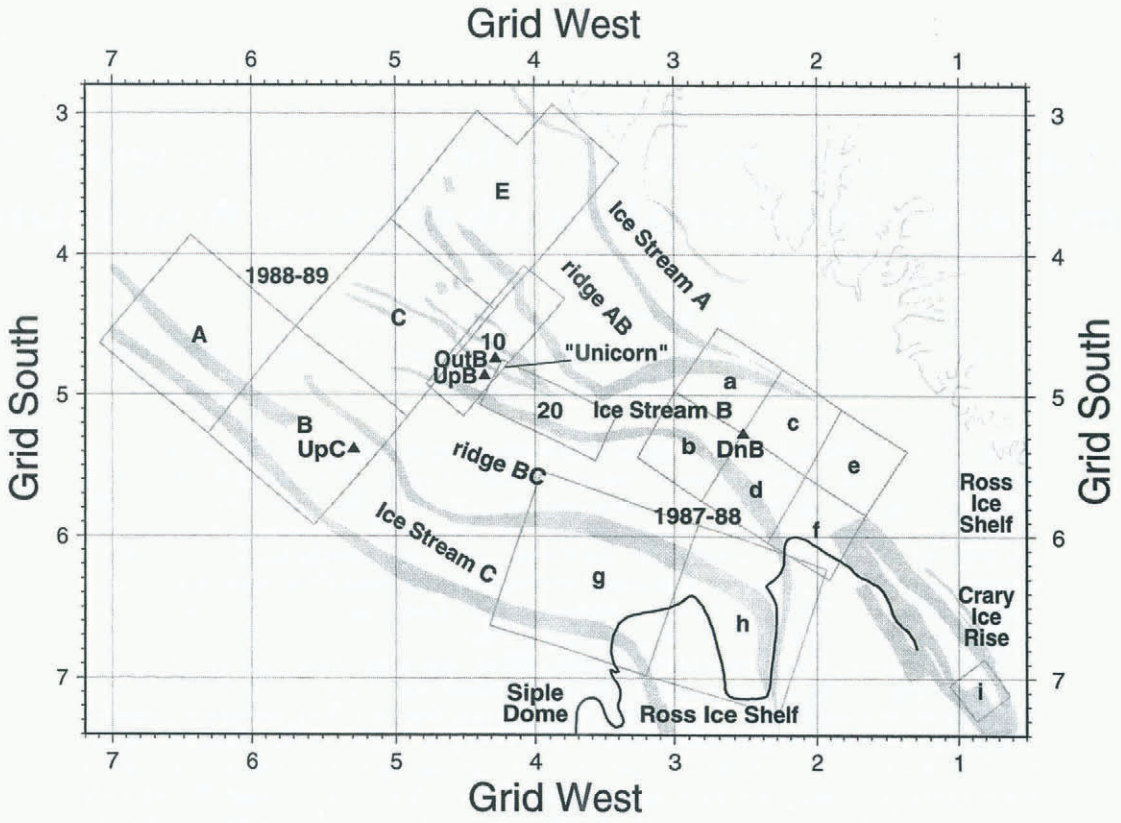

Fig. 1. Map of the Siple Coast Project study region, showing 1987–88 and 1988–89 airborne radar coverage. Flights in 1987–88 (this paper) covered the nine blocks a–i. Flights in 1988–89 (Retzlaff and others, 1993) covered six blocks: A, B, C, E, 10 and 20. The heavy line denotes the grounding line. The origin of the rectangular grid coordinate system used on this and subsequent maps is at the South Pole; grid north is toward Greenwich and therefore toward the top of the map. Squares have sides of length equal to 1° of latitude. The boundaries of the glaciological features are taken from Shabtaie and Bentley (1987).

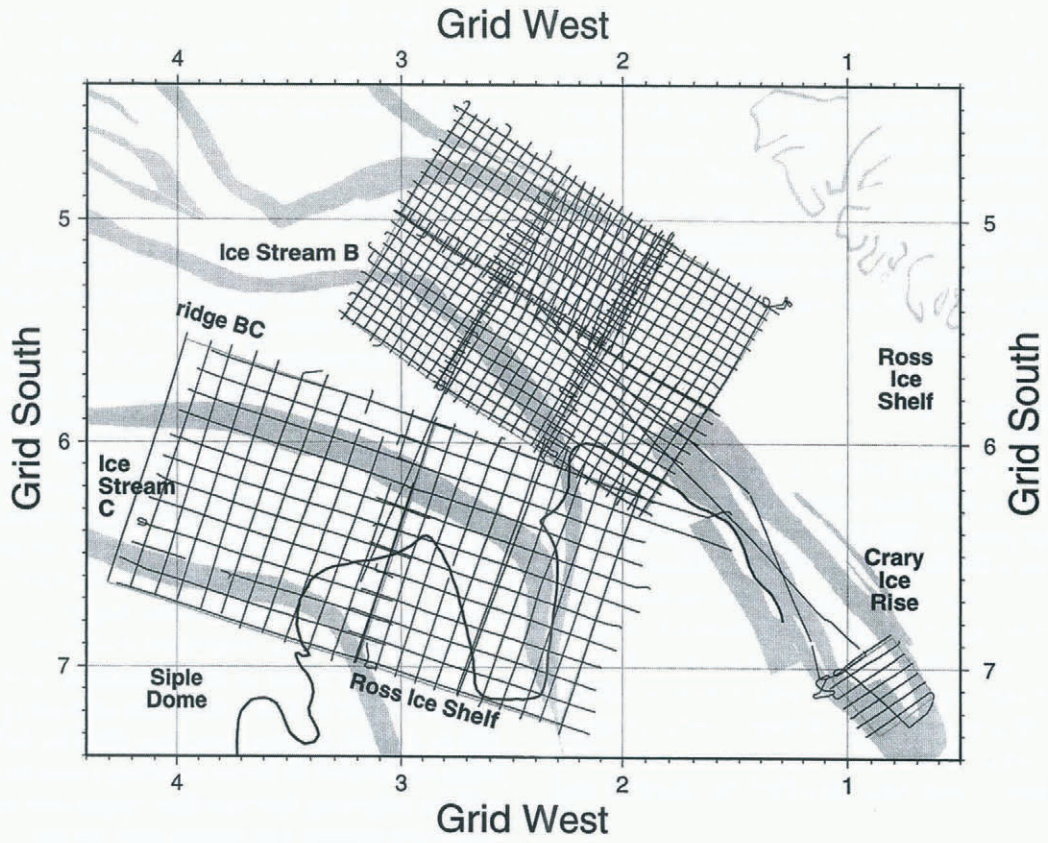

Fig. 2. Map of the nine blocks in the 1987–88 survey, showing all the radar-sounding flight-lines. The transects along which the reflection-strength profiles of Figure 3 were drawn are indicated by the thinner hachured line segments; those along which the averages of Figure 6 were taken are indicated by the wider hachured segments.

navigation system drift. The 32 flight closures for the whole survey have a mean of 2.9 km and a standard deviation of 1.9 km, with a maximum closure of 7.4 km. Navigational errors of 1 or 2 km are also indicated by the positions recorded when passing over or near satellite-surveyed ground stations. Corrections to each flight were applied on the basis of an assumed linear drift with time.

Crossover corrections

The crossover errors for ice thickness (differences in measured values where two flight-lines cross) were used first to evaluate the effectiveness of the linear drift correction for navigation. Generally speaking, the standard deviation in ice-thickness crossover differences was substantially reduced by application of the drift correction in blocks where it was initially large (e.g. from 28 to 20 m (30%) for block a), whereas small standard deviations tended actually to be increased (e.g. from 6 to 8 m (33%) in block h). Overall, the standard deviation was decreased by 13%. Crossover errors remaining after the drift correction were then removed by linear distribution of the errors within each transect segment between two crossing points.

Interpolation

For mapping, the data had to be interpolated from their distribution every 60 m along widely spaced transects to an evenly spaced grid. A minimum-curvature gridding program was used for this, although two other interpolation methods (kriging and inverse-distance) were considered. Minimum curvature is very fast and produced smooth contour lines that enhanced the trends of topographic features. (Kriging produced slightly better maps but took much longer to compute.) The data were gridded at a density of one grid point every 1.11 km (0.01° of latitude). No smoothing was performed on the data after they were gridded. A standard public-domain contouring routine (Generic Mapping Tools) was applied to the gridded data to produce the ice-thickness map.

Basal-reflection strength

The basal-reflection strength, P_s, is the difference between the actual power in the basal echo, P_e, and a model for the received power, P_r, that uses the aircraft height above the ice, the ice thickness and the equipment calibrations to compensate for geometrical spreading, dielectric absorption and the receiver gain function. The model is given by

$$P_r = (P_{tx} + P_{rx} + P_{tvg}) - (R_g + R_t + T_a + S_v + S_b) \quad (1)$$

where P_{tx} is the transmitted power (500 W), P_{rx} is the gain before the calibration-insertion point of the system (includes transmit/receive-switch and feed-cable loss), P_{tvg} is the receiver gain after the calibration-insertion point, R_g is the geometrical spreading loss, given by

$$R_g = 20 \log \frac{8\pi(h_a + h_i/n)}{\lambda G}, \quad (2)$$

h_a is the aircraft height, h_i is the ice thickness, n is the index of refraction (1.75), λ is the wavelength in air (6 m at 50 MHz), G is the antenna gain (6 dB), R_t is the loss due to dielectric absorption in the ice column, T_a is the transmission loss at the ice–air boundary (about 1 dB), S_v is the loss due to small-scale volume scattering in ice (about 6 dB), and S_b is the scattering loss due to a rough ice–rock interface (about 0 dB). This model is adapted from the one used by Shabtaie and others (1987), from whom we also obtained the numerical values cited. The P_{tvg} term was added because the radar system used in 1987–88 had a time-varying gain that provided more gain later in the record to compensate for the increasingly weak echoes.

The numerical value of the dielectric absorption, R_t, is not well known, both because the temperature in the ice column is not measured and because the temperature coefficient of absorption itself is not well determined, perhaps owing to a general failure in the literature to take varying impurity concentrations into account (Corr and others, 1993). We therefore follow the procedure used by Shabtaie and others (1987) and assume that the strongest reflections have a relative reflection strength of 0 dB. In our survey, the strongest echoes are found from the base of the ice shelf in front of Ice Stream C, a location where the reflection coefficient, from sea water, is maximal (theoretical reflectivity −0.6 dB). This leads to a value for R_t of 17.3 dB km^{-1}, a reasonable value (cf. Shabtaie and others, 1987).

Measurements of raw received power, averaged over 1 km segments of flight line, are accurate to about 1 dB, the standard deviation of the values within a single segment. All the parameters in Equation (1) except R_t can be considered constant across our survey (the error in R_g that arises from uncertainties in h_a and h_i is less than 0.1 dB). Lateral variations in basal-reflection strengths (Fig. 3), as finally calculated, therefore reflect a combination of variations in the reflecting characteristics of the bed, which depend on its roughness and the impedance contrast between the ice and the bed, deviations of actual absorption in the ice from that assumed, and scattering of the downgoing and upgoing signals by large-scale disturbances within the ice (principally near-surface crevasses), to an accuracy of about ±1 dB.

ERROR ANALYSIS FOR ICE THICKNESS

Ice-thickness errors were analyzed using the procedure described by Retzlaff and others (1993). The component errors were: from migration of the reflection point, <1 m (the average bed slope in the survey area is 2×10^{-3}); from positioning errors, 5 m; from the auto-picker, 7 m; from the radio-wave speed, 5 m; and from interpolation, 15 m. The combined (root sum square) error is 20 m at interpolated points, and 11 m at points along the flight-lines. The latter is close to the average crossover residual for the ice thickness in blocks a–h, which is 12 m.

MAPS

The corrected data were combined into datasets that included all nine blocks, and maps were created of ice thickness and basal-reflection strength (Figs 4 and 5). Features of the ice-thickness map delineated by only one contour line should be treated with caution. In particular, a small circle or oval that lies on only one flight-line is most likely an artifact of the contouring routine that does not depict the real topography or thickness accurately. It would take only a small redrafting of individual contour lines in Figure 4, which could be done without violating any of the data, to make open features out of closed ones.

https://doi.org/10.3189/S0022143000002434 Published online by Cambridge University Press

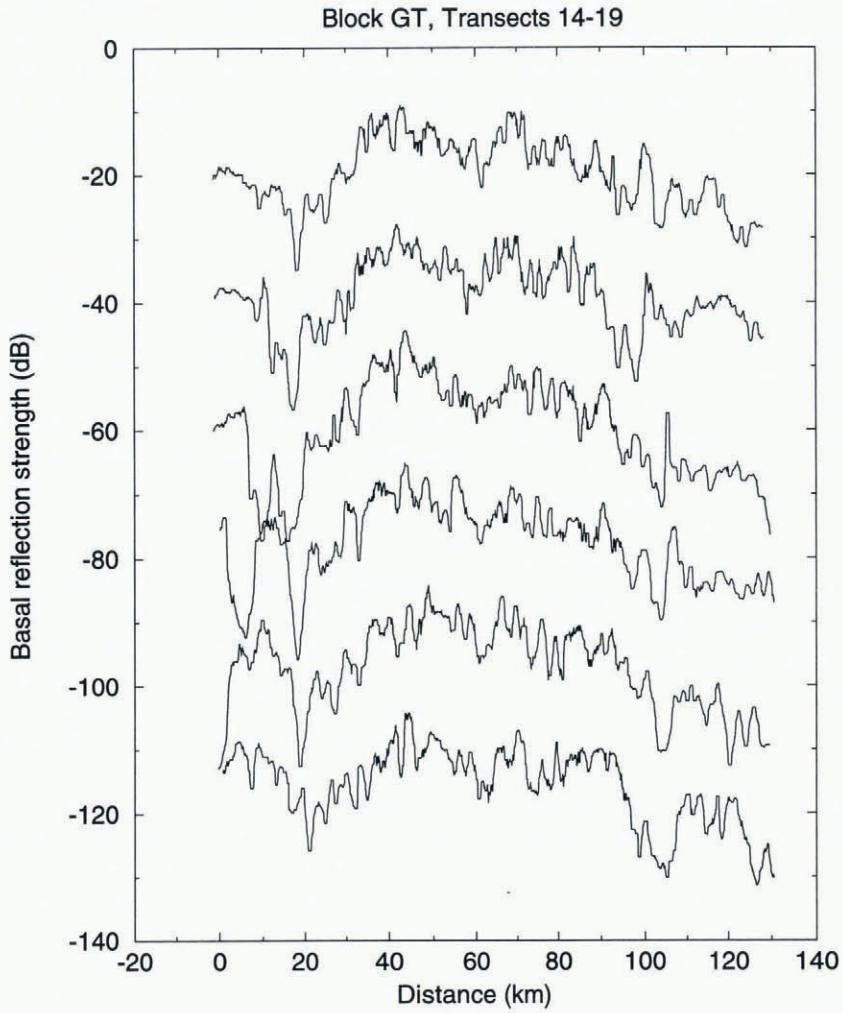

Fig. 3. Sample profiles of basal-reflection strength, calculated along six transects across Ice Stream C (see Fig. 2 for the locations of the transects). The reflection-strength scale applies to the top (grid westernmost) profile; the other profiles have been translated successively downward by 20 dB for clarity.

DISCUSSION

Ice-thickness map

The map of ice thickness that results from these high-density surveys (Fig. 4) is remarkably similar to the map previously produced from reconnaissance surveys (Shabtaie and Bentley, 1988). Our analysis so far has revealed no significant differences between the two, so we will not discuss this map further here.

Reflection-strength map

As stated above, the reflection-strength map (Fig. 5) can be expected to depict variations in four quantities: basal reflectivity (a function of the impedance contrast), absorption in the ice, scattering from crevasses, and basal roughness (Robin and others, 1969). We believe that the first three factors enter significantly into the variations seen in the map; the fourth is unlikely to contribute more than a few dB for a realistically rough surface and an outgoing pulse longer than ~0.2 (Robin and others, 1969); the outgoing pulse length in our system is 0.3.

The reflection strengths P_s not only vary widely across the map, but also show strongly regional characteristics. We will examine the differences between four regions: Ice Stream B, Ice Stream C, ridge BC and the Ross Ice Shelf; to quantify those differences we have calculated the statistical characteristics of P_s along representative transects across each (Fig. 6 and Table 1; see Fig. 2 for locations of the transects). We will examine Crary Ice Rise separately, because the glaciological conditions there change so rapidly in short distances that the statistical approach is not very helpful.

The strongest reflections, not surprisingly, come from the Ross Ice Shelf. (We have only considered the portion of the Ross Ice Shelf in front of Ice Stream C, because of uncertainty as to just where the grounding line really is between the Ross Ice Shelf and Ice Stream B (Shabtaie and Bentley, 1987; Bindschadler, 1993). The mean of P_s is −5 dB (Table 1); the peak in the distribution curve is at about −3 dB (Fig. 6). The distribution is strongly skewed, which we interpret to mean that there are several factors that can diminish P_s from the ideal obtained from a smooth reflector through ice without scattering losses — buried crevasses, a rough, mushy or unfavorably shaped interface, basal freeze-on of sea ice — but little that can enhance it. The absolute value of P_s is not significant; it simply represents a bias of about 2.5 dB (the difference between −3 dB and the theoretical reflection loss from a boundary between ice and sea water of −0.5 dB) in our calibrating assumption that the strongest reflection was at 0 dB.

On the grounded ice, the reflection-strength distribu-

https://doi.org/10.3189/S0022143000002434 Published online by Cambridge University Press

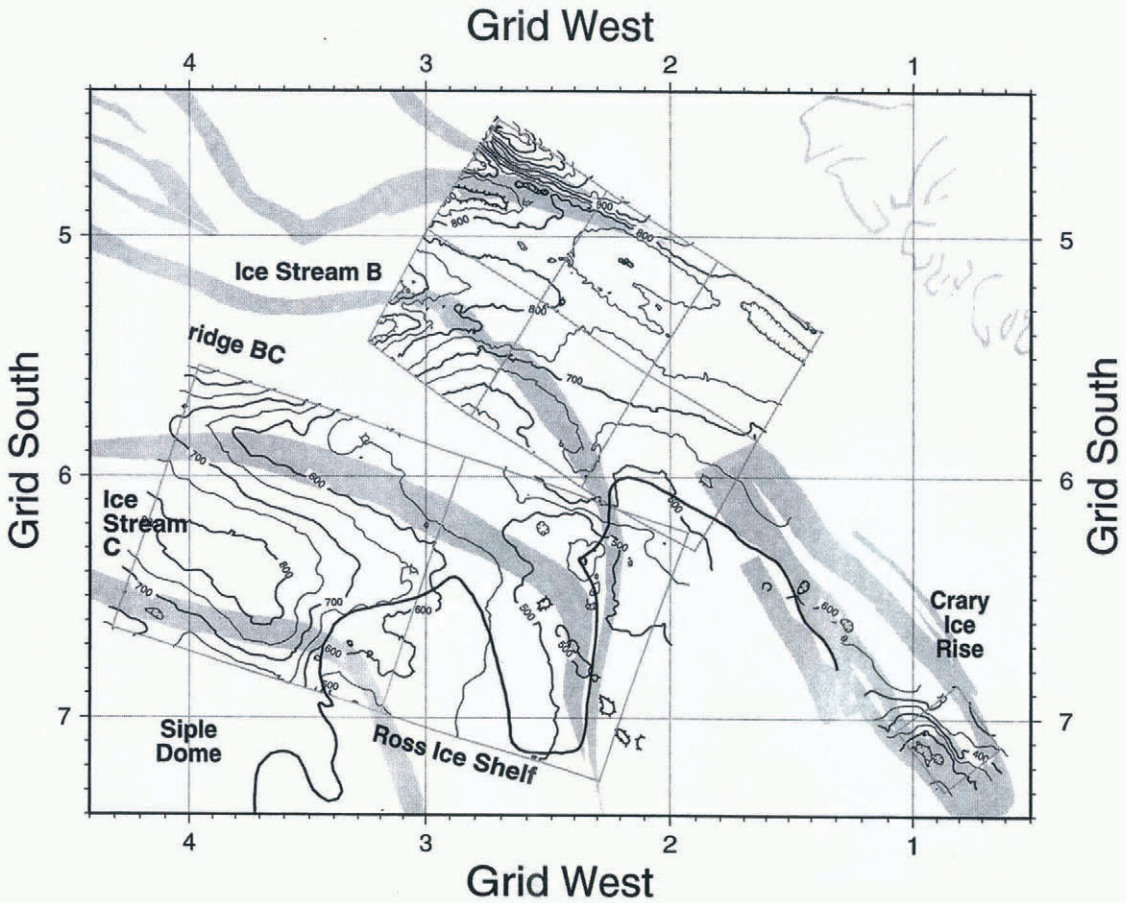

Fig. 4. Ice-thickness map from the 1987–88 survey. The contour interval is 50 m. The borders of the ice streams (from Shabtaie and Bentley, 1987) are shaded.

tions are approximately normal (Fig. 6). The mean difference in P_s between the Ross Ice Shelf and Ice Stream C is 8 dB, of which 3 dB can be attributed to the difference between the reflection coefficients from sea water and fresh water, respectively (Shabtaie and others, 1987). The other 5 dB loss presumably is the effect of the subglacial sediment. (It is unlikely that there is any significant difference in the scattering losses from buried crevasses between Ice Stream C and the immediately downstream part of the Ross Ice Shelf, since the latter flows from the former.) Shabtaie and others (1987) showed evidence for the pooling of water in some regions under Ice Stream C and its absence in other places; our results here accord with theirs, which may indeed explain the patchy character of P_s on Ice Stream C.

It is noteworthy that the decrease in P_s between the Ross Ice Shelf and Ice Stream C is gradual, particularly across the grid south-central part of the grounding line (Fig. 5). This suggests that sea water may penetrate some distance inland from the grounding line, as suggested also by the recent observation of a tidal influence on subglacial earthquakes on Ice Stream C (Anandakrishnan and Alley, 1997). (Although Anandakrishnan and Alley (1997) discount propagation of the tidal influence in a subglacial water film because it would have to be several cm thick to produce the observed propagation speed, we note that Shabtaie and others (1987) calculated just such a thickness for the water in the subglacial pools.) It is clear that the bed of Ice Stream C is not frozen, because if it were, P_s should decrease by some 20 dB (Jiracek, 1967). Apparently, the stagnation of Ice Stream C was not caused by its freezing to its bed. (This observation does not contradict either of the existing theories for the stagnation; both involve diversion of excess water, either into Ice Stream B (Alley and others, 1994) or into channeled flow (Retzlaff and Bentley, 1993), but neither implies that the bed then froze.)

The average P_s on Ice Stream B is 7 dB less than on Ice Stream C. Since the beds of both are unfrozen, the difference must be attributable to some combination of crevasse scattering on Ice Stream B and differential absorption.

Absorption depends principally on temperature and impurities in the ice. It is unlikely that impurity levels vary much across the area mapped in this study. To begin with, the two ice streams draw their ice from the same interior region of the ice sheet. Furthermore, ridge BC is about the same distance as that interior region from the ocean north of Marie Byrd Land, the principal source of the moisture that precipitates in western West Antarctica (Bromwich, 1984), so the ice there too probably has a similar concentration of ionic impurities, which come mainly from the ocean (Corr and others, 1993). Direct evidence for similar impurity levels comes from Langway and others (1974) who found from measurements in a core from the Ross Ice Shelf that there was no consistent trend in cation concentrations with depth in the deeper part of the core, wherein depth is a proxy for distance inland from the grounding line. We will assume, therefore, that varying impurities do not cause significant differences in absorption between our sites.

As for temperature, there are, unfortunately, no actual measurements in the area of this survey; the closest are some 200 km upstream. Temperatures have been measured through the entire ice column at station UpB on Ice Stream B2, at station UpC on Ice Stream C, and at several sites on ridge B1/B2 (the "Unicorn", Fig. 1) (Engelhardt and Kamb, 1994; personal communication from H. Engelhardt, 1997). At

https://doi.org/10.3189/S0022143000002434 Published online by Cambridge University Press

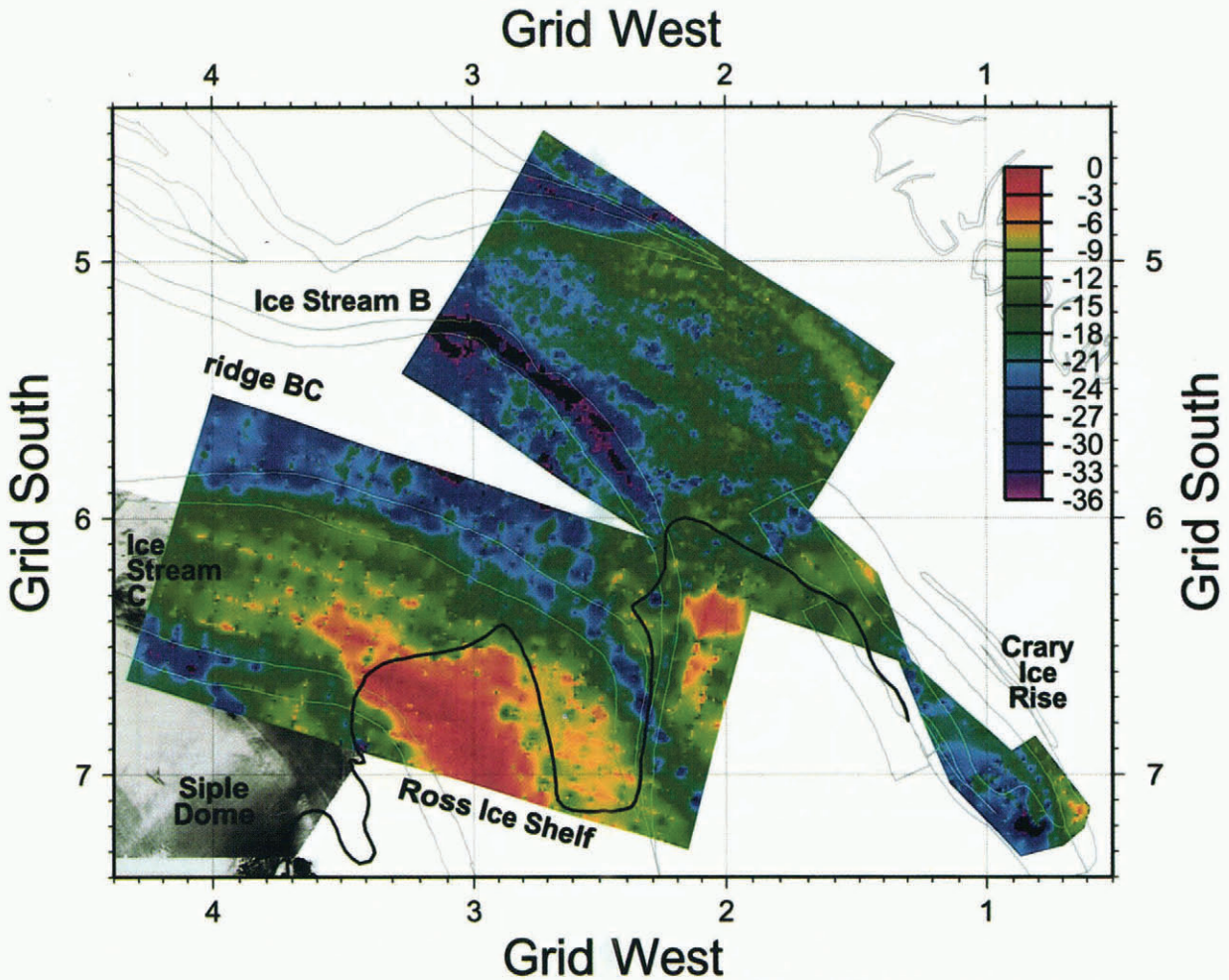

Fig. 5. Map of basal-reflection strength, in dB relative to an assumed value of 0 dB on the Ross Ice Shelf in front of Ice Stream C. The color scale is shown in the figure. The borders of the ice streams as mapped by Shabtaie and Bentley (1987) are shown by thin lines. In the lower left corner, part of a Landsat image of Siple Dome and the northern portion of Ice Stream C (kindly provided by R. A. Bindschadler, personal communication, 1997) has been superimposed.

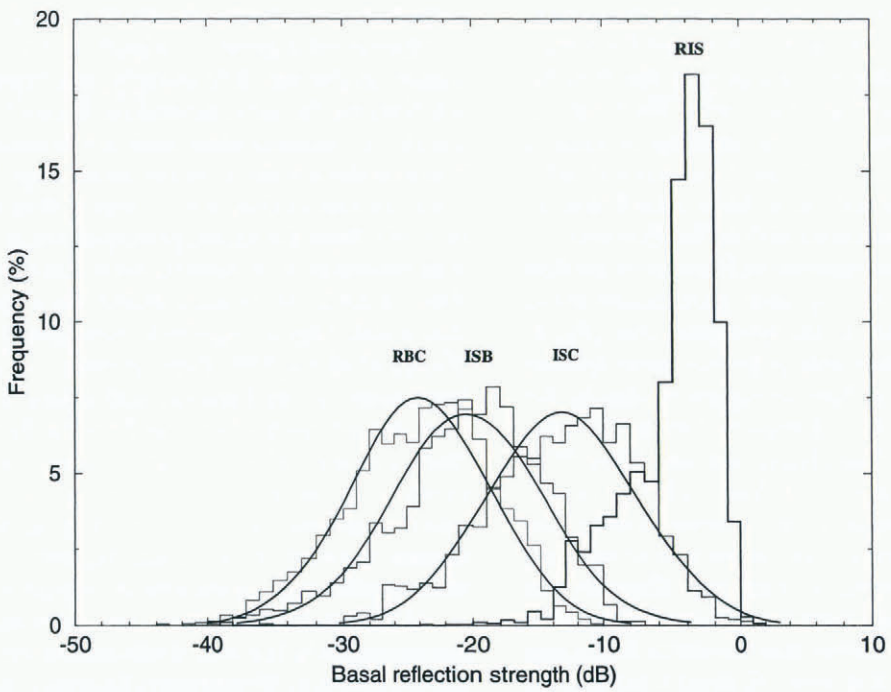

Fig. 6. Normalized histograms of basal-reflection strengths from representative transects (Fig. 2) across ridge BC (RBC), Ice Stream B (ISB), Ice Stream C (ISC) and the Ross Ice Shelf (RIS). Normal distribution curves with the parameters given in Table 1 have been fitted to the first three histograms but not to that for RIS, which is clearly not normally distributed.

https://doi.org/10.3189/S0022143000002434 Published online by Cambridge University Press

Table 1. Regional characteristics of basal-reflection strengths

Location	Number of points	Maximum	Reflection strengths (dB) Minimum	Median	Mean	Standard deviation
Ridge BC	1828	−10	−53	−23.6	−24.1	5.3
Ice Stream B	2074	−8	−43	−19.9	−20.5	5.7
Ice Stream C	1945	+2	−35	−12.8	−13.3	5.6
Ross Ice Shelf	2773	+1	−38	−4.0	−5.0	3.6

those upstream sites, the ice is colder at all depths (except near the surface) on the ridge than it is at the same relative depths on Ice Stream B; the temperatures at UpC are intermediate, but closer to those on the ridge. We have calculated the total absorption through the ice columns at the three locations, based on the assumption that the absorption constant varies in proportion to $e^{-E/RT}$, where T is the absolute temperature, R is the gas constant and E is the activation energy (taken to be 80 kJ mol^{-1} from a fit to experimental data given by Johari and Charette (1975)). We find that the total two-way absorption is the least on ridge B1/B2, 2 dB more at UpC and 8 dB more still at UpB. If these differences are transferred downstream unchanged (we believe it likely that the temperature difference is associated with the widely different dynamic activity of the two ice streams and therefore would persist downstream), they imply that the smaller P_s values on Ice Stream B than on Ice Stream C could be caused entirely by the greater absorption in the warmer ice of Ice Stream B. The younger but still well-buried crevasses on Ice Stream B apparently do not cause significantly greater scatter than those on Ice Stream C.

Basal-reflection strengths on ridge BC are 11 dB less, on average, than on Ice Stream C. Since ridge BC is free of crevasses (Rose, 1979; Shabtaie and Bentley, 1987; Shabtaie and others, 1987; Retzlaff and Bentley, 1993), the two factors to consider in this case are the dielectric absorption and the reflectivity of the bed. But the results from upstream, if ridge B1/B2 is a valid analog to ridge BC, suggest that ridge BC should be slightly colder than Ice Stream C; it is most unlikely that it is the 4°C or so warmer that would be needed to produce an additional 11 dB absorption loss. Thus we attribute the weak reflections from the bed of ridge BC to a small basal reflection coefficient.

The loss upon reflection from a boundary between ice and frozen sediments varies widely, at least between 10 and 30 dB, depending on the type of sediment (Jiracek, 1967, table 5). That range is enough to explain the low reflectivities on the ridge if the bed there is frozen, even after allowing for the possibility of a lesser absorption on the ridge because of lower temperatures. If the bed were wet, on the other hand, it would be very difficult to explain a reflection coefficient of −20 dB or weaker. We consider it much more likely that the ice on ridge BC is frozen to its bed, as it is on ridge B1/B2 (personal communication from H. Engelhardt, 1997).

Bands with losses greater than 30 dB are closely associated with the previously mapped margin of Ice Stream B (Fig. 5), as would be expected as a result of extreme scattering in the highly disturbed ice of the marginal shear zones.

Surprisingly, such is not the case with Ice Stream C. On the grid-northern side of the ice stream, grid west of about 2.6° W (grid), the center of the mapped shear margin is associated with a strong gradient in reflection strength, from stronger under Ice Stream C to weaker under ridge BC, not with a minimum. We interpret this as being the boundary between the wet bed under Ice Stream C and the frozen bed under ridge BC. If that is correct, it suggests a cause-and-effect relationship, although it is not clear whether the ice-stream margin was there because it was the boundary of the frozen bed, or it was the position of the ice stream that determined where the bed was frozen. We also conclude from the absence of a minimum in reflection strength that even the crevasses in the marginal shear zone of this stagnant ice stream have healed to the point that they produce only weak scattering.

The grid southern margin of Ice Stream C is not marked by any reflection-strength signal, grid east of grid 3.8° W. In this area we believe the bed is unfrozen on both sides of the ancient shear margin. Around grid 4° W there is an intriguing suggestion that a reflection-strength minimum marks the boundary farther upstream and then splits into two forks, one associated for a short distance with the mapped shear margin of the ice stream and one with the "scar" on the flank of Siple Dome, clearly seen in the Landsat image (pasted into Fig. 5) that has been attributed to another former shear margin by Stephenson and Bindschadler (1990). Unfortunately, only short segments of the "scar" and the ice-stream margin upstream from the junction lie within the boundaries of the reflection-strength map.

Weak reflections are associated with the main body of Crary Ice Rise (around grid 7° S, 1° W), presumably because the bed is frozen (Bindschadler and others, 1990). The grid northeastern boundary of the ice rise is sharply delineated by a contrast in reflection strength, with the stronger echoes coming from the base of the ice shelf to the grid northeast. The very weak reflections south of Crary Ice Rise are the result of the highly disturbed ice in the "wake" of the ice rise. The long "tail" of the ice rise that extends grid northwestward toward Ice Stream B is poorly defined by Figure 5, because there are only two, nearly parallel flight-lines in that area (Fig. 2); in any case, the actual boundaries of the ice rise are not themselves well known (Shabtaie and Bentley, 1987; Bindschadler, 1993).

In several instances there are substantial deviations between the mapped positions of the ice-stream boundaries, where they approach and enter the Ross Ice Shelf, and the reflection-strength features that appear to be associated with them (Fig. 5). Careful examination of all the data (new and old) and comparison with satellite images probably would yield an explanation. We leave this for a future investigation.

CONCLUSIONS

From maps of ice thickness and basal-reflection strength based on more than 17 000 km of high-quality digital airborne radar data collected over the downstream portions of Ice Streams B and C, we conclude the following.

1. Ice thickness varies gradually across the area; the new high-spatial-density coverage has not revealed any features not already known from reconnaissance mapping.
2. The principal new information comes from the map of basal-reflection strength, from which we conclude that

https://doi.org/10.3189/S0022143000002434 Published online by Cambridge University Press

(a) near-surface scattering is weak except from the highly disturbed ice in the shear margins of Ice Stream B;

(b) the bed of ridge BC is frozen;

(c) the bed of Ice Stream C is unfrozen;

(d) the boundary between the frozen and unfrozen beds beneath ridge BC and Ice Stream C, respectively, lies below the former shear margin that separates them; and

(e) the basal unfrozen boundary between ridge BC and Ice Stream B is obscured by other reflection-strength changes associated with the marginal shear zone and a marked change in englacial temperature.

ACKNOWLEDGEMENTS

The authors wish to thank the other members of the University of Wisconsin field party, especially D. B. Blankenship and L. A. Powell, for invaluable assistance in collecting the data. The Twin Otter was supplied, under contract from the U.S. National Science Foundation (NSF), by Ken Borek Air, Ltd, of Calgary. We are grateful for the high degree of cooperation from the Ken Borek crew. This work was supported by the NSF grant DPP86-14011. This is contribution No. 576 of the University of Wisconsin–Madison, Geophysical and Polar Research Center.

REFERENCES

Alley, R. B., S. Anandakrishnan, C. R. Bentley and N. Lord. 1994. A water-piracy hypothesis for the stagnation of Ice Stream C, Antarctica. *Ann. Glaciol.*, **20**, 187–194.

Anandakrishnan, S. and R. B. Alley. 1997. Tidal forcing of basal seismicity of Ice Stream C, West Antarctica, observed far inland. *J. Geophys. Res.*, **102**(B7), 15,183–15,196.

Bindschadler, R. 1993. Siple Coast Project research of Crary Ice Rise and the mouths of Ice Streams B and C, West Antarctica: review and new perspectives. *J. Glaciol.*, **39**(133), 538–552.

Bindschadler, R. A., E. P. Roberts and A. Iken. 1990. Age of Crary Ice Rise, Antarctica, determined from temperature–depth profiles. *Ann. Glaciol.*, **14**, 13–16.

Bromwich, D. H. 1984. Precipitation regime of the West Antarctic ice sheet. *In* Van Loon, H., *ed. Environment of West Antarctica: potential CO_2-induced changes*. Washington, DC, National Academy Press. National Research Council. Polar Research Board. Committee on Glaciology, 107–115.

Corr, H., J. C. Moore and K. W. Nicholls. 1993. Radar absorption due to impurities in Antarctic ice. *Geophys. Res. Lett.*, **20**(11), 1071–1074.

Engelhardt, H. and B. Kamb. 1994. Vertical temperature profile of Ice Stream B. *Antarct. J. U.S.*, **28**(5), Review 1993, 63–66.

Jiracek, G. R. 1967. Radio sounding of Antarctic ice. *Univ. Wis. Geophys. Polar Res. Cent. Res. Rep. Ser.* 67-1.

Johari, G. P. and P. Charette. 1975. The permittivity and attenuation in polycrystalline and single-crystal ice Ih at 35 and 60 MHz. *J. Glaciol.*, **14**(71), 293–303.

Langway, C. C., Jr, M. Herron and J. H. Cragin. 1974. Chemical profile of the Ross Ice Shelf at Little America V, Antarctica. *J. Glaciol.*, **13**(69), 431–435.

Retzlaff, R. and C. R. Bentley. 1993. Timing of stagnation of Ice Stream C, West Antarctica, from short-pulse radar studies of buried surface crevasses. *J. Glaciol.*, **39**(133), 553–561.

Retzlaff, R., N. Lord and C. R. Bentley. 1993. Airborne-radar studies: Ice Streams A, B and C, West Antarctica. *J. Glaciol.*, **39**(133), 495–506.

Robin, G. de Q., S. Evans and J. T. Bailey. 1969. Interpretation of radio echo sounding in polar ice sheets. *Philos. Trans. R. Soc. London, Ser. A*, **265**(1166), 437–505.

Rose, K. E. 1979. Characteristics of ice flow in Marie Byrd Land, Antarctica. *J. Glaciol.*, **24**(90), 63–75.

Schultz, D. G., L. A. Powell and C. R. Bentley. 1987. A digital radar system for echo studies on ice sheets. *Ann. Glaciol.*, **9**, 206–210.

Shabtaie, S. and C. R. Bentley. 1987. West Antarctic ice streams draining into the Ross Ice Shelf: configuration and mass balance. *J. Geophys. Res.*, **92**(B2), 1311–1336. (Erratum: *J. Geophys. Res.*, 1987, **92**(B9), 9451.)

Shabtaie, S. and C. R. Bentley. 1988. Ice-thickness map of the West Antarctic ice streams by radar sounding. *Ann. Glaciol.*, **11**, 126–136.

Shabtaie, S., I. M. Whillans and C. R. Bentley. 1987. The morphology of Ice Streams A, B, and C, West Antarctica, and their environs. *J. Geophys. Res.*, **92**(B9), 8865–8883.

Stephenson, S. N. and R. A. Bindschadler. 1990. Is ice-stream evolution revealed by satellite imagery? *Ann. Glaciol.*, **14**, 273–277.

MS received 30 June 1997 and accepted in revised form 17 November 1997